A new approach to compensate for illumination differences in 4D surveys with different individual acquisition geometries

Didier Lecerf[1*] and Martin Besselievre[2] demonstrate how the concept of Point Spread Functions can be successfully applied to time-lapse seismic when the respective acquisition geometries are very different and cannot be closely repeated.

Introduction

Successful time-lapse (or 4D seismic) studies require special care when it comes to the removal of undesirable artifacts caused by the differences in acquisition geometries. By attempting to repeat the source and receiver geometries between surveys as precisely as possible any subsequent 4D noise is minimized so that subtle seismic signal variation induced by reservoir production can be detected. It is commonly accepted that the required repeatability accuracy is directly linked to the desired sensitivity and resolution of the 4D signal. Illumination studies prior to any 4D experiments ensure that the reservoir is illuminated in as identical a fashion as possible between base and monitor survey so that the desired 4D effects can be recovered. In fact, it is common practice to plan and design 4D surveys with optimal acquisition repeatability in mind.

However, in some cases it is not possible to repeat the survey geometries between vintages. When the geometry differences are small, corrections can be made during data processing by including steps such as 4D binning, which aim to preserve those seismic traces that are associated with the smallest variation in source and receiver positions. The process of 4D binning is particularly effective when the acquisition for both the base and monitor survey are very similar such as streamer on streamer or OBS (Ocean Bottom Seismic) on OBS surveys. Nevertheless, 4D binning does not perform well when both acquisition vintages comprise significant differences in their respective source and receiver positions. This is for example the case when different streamer acquisition azimuths are involved or when large cable feathering differences at long offsets are observed or indeed when a towed streamer survey is to be compared with an OBS acquisition.

Correction for significant acquisition geometry difference in time-lapse seismic

Some solutions to this problem have been described in the literature for implementations in both the data and image domain. For reconciling steamer and OBS data, intelligent 4D binning in the data domain for example can be performed by selecting trace pairs based on multiple criteria such as the Common Depth Point (CDP) distance and/or pseudo-incidence angle and azimuth similarities at the reservoir level (Lecerf et al., 2010). Alternatively, wavefield propagation can be used to re-datum the different vintages to the same sea level before the 4D binning is applied. But this method requires very dense spatial sampling of the source and/or receiver locations and has limitations when large differences between the recording datum exist such is the case between OBS and towed streamer surveys in a deep water context. To minimize illumination differences in the image domain, Thierrot et al. (2015) recommend matching the migrated data in the common incidence angle and/or common azimuth domain. Dip-angle image filtering has also been suggested in order to better reconcile towed streamer and OBN migrated images (Haacke et al., 2017).

The image domain approach for correcting illumination differences between 4D datasets that we are presenting here builds on previously published work concerning wave equation reflectivity inversion using Point Spread Functions (PSFs). In this two-step least-squares imaging method, the reflectivity of depth migrated images is recovered by explicitly computing multi-dimensional PSFs using wave-equation modeling and deconvolving these PSFs with the final migrated image (Valenciano et al., 2006). Ayeni and Biondi (2010) have previously exploited the PSF concept for 4D reservoir monitoring using a target-oriented joint least-squares migration/inversion approach. They demonstrated that using joint inversion with spatial and temporal constraints enables the recovery of the reflectivity variations consistent with a reservoir production scenario.

The aim of the study presented here is to highlight the benefit of the joint inversion in the image domain and to define a 4D formulation which is not dependent on geological and/or reservoir production constraints.

Combining PSFs from different 4D datasets

We are extending and modifying the previous joint inversion formulations for 4D reservoir monitoring by introducing the concept of cross-survey PSFs (XPSFs). The term cross-survey here refers to the illumination contribution that is common to two or more surveys used in a 4D experiment. This is achieved by 'mixing' the PSFs of the individual surveys through the joint inversion such that common components of the 3D PSF fields associated with common illumination are enhanced and uncorrelated elements

[1] PGS | [2] Geokinetics, formerly PGS
* Corresponding author, E-mail: didier.lecerf@pgs.com

are suppressed. The result of this process is a consistent 4D reflectivity cube.

When acquisitions are repeated closely, 4D binning processes may deliver a similar outcome to the proposed jointly inverted 4D image using XPSFs in terms of common illumination. Selecting trace pairs with similar ray paths during the trace binning process ensures that a comparable illumination at the reservoir level is achieved during migration.

The benefit of working in the image domain, as proposed here, through the use of joint reflectivity inversion is that the illumination variation can be directly evaluated and compensated for at any location in the 4D image regardless of acquisition geometries. In addition, the multi-dimensional deconvolution should increase and stabilize the spatial resolution of the true production-related 4D effects.

4D reflectivity inversion using XPSFs

As shown by Valenciano et al. (2006), a least-squares inversion framework can be used for inverting the reflectivity in the image domain.

The recorded seismic data **d** can be expressed as a linear modelling operator **L** working on the subsurface reflectivity **r.**

$$d = Lr$$

The reflectivity **r** therefore can be estimated using the Hessian matrix **H = L'L,** where **L'** is the migration operator (or adjoint to the modelling operator).

$$\hat{r} = \left(L'L\right)^{-1} L'd_{obs} = H^{-1}m_m$$

$\hat{r} = estimated\ reflectivity$

$d_{obs} = observed\ data$

$m_m = migrated\ image$

The main difficulty of solving the above equation is the need to explicitly compute the inverse of the Hessian matrix. This matrix can be very large for most imaging problems and is therefore commonly estimated using a least-squares inversion methodology.

Using PSFs, the Hessian H can be very efficiently computed in a target-oriented fashion as a set of local imaging responses of a grid of scatter points.

Separate reflectivity inversion for base and monitor surveys

In a 4D time-lapse experiment a matrix system for separate inversions can be set as follows, using $\hat{r}_0, \hat{r}_1$ and $\tilde{m}_0, \tilde{m}_1$ respectively, to estimate reflectivity models and migrated images for the base and monitor surveys:

$$\left(H_0 + \varepsilon_0\right).\hat{r}_0 = \tilde{m}_0\ for\ the\ base.$$

$$\left(H_1 + \varepsilon_1\right).\hat{r}_1 = \tilde{m}_1\ for\ the\ monitor.$$

4D joint reflectivity inversion summary

Rather than performing reflectivity inversions separately for the base and monitor surveys it would be more meaningful to estimate the reflectivity from the combined dataset to represent the true 4D reflectivity. This is achieved by setting up a joint inversion system (with no temporal/geological constraints) as described below:

$$\left(\begin{bmatrix} H_0 & 0 \\ 0 & H_1 \end{bmatrix} + \begin{bmatrix} \varepsilon_0 & 0 \\ 0 & \varepsilon_1 \end{bmatrix}\right)\begin{bmatrix} \hat{r}_0 \\ \hat{r}_1 \end{bmatrix} = \begin{bmatrix} \tilde{m}_0 \\ \tilde{m}_1 \end{bmatrix}$$
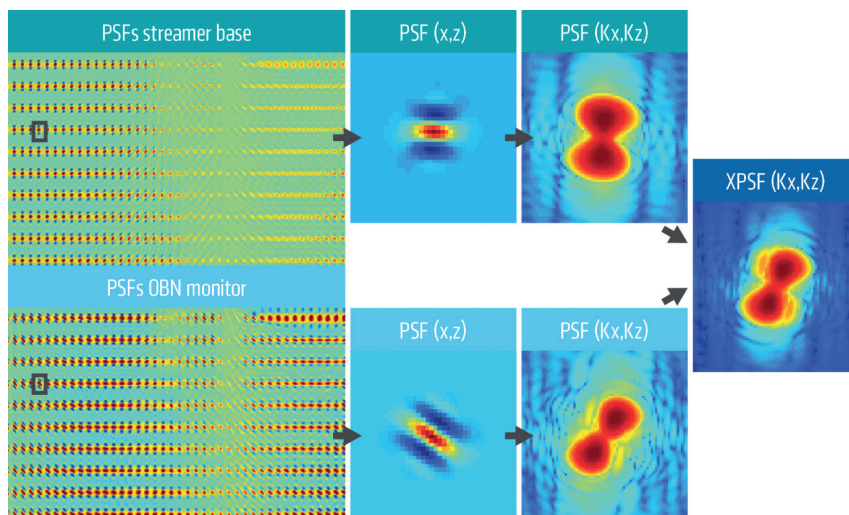
$$regularisation\ terms: \quad \varepsilon_0 = \lambda_0 \left\langle \mathbf{H}_0^* \mathbf{H}_0 \right\rangle and\ \varepsilon_1 = \lambda_1 \left\langle \mathbf{H}_1^* \mathbf{H}_1 \right\rangle$$

By introducing the cross-survey Hessian term H_1H_j, the system can be rewritten:

$$\left(\begin{bmatrix} H_1H_0 & 0 \\ 0 & H_0H_1 \end{bmatrix} + \begin{bmatrix} \varepsilon_{01} & 0 \\ 0 & \varepsilon_{10} \end{bmatrix}\right)\begin{bmatrix} \hat{r}_0 \\ \hat{r}_1 \end{bmatrix} = \begin{bmatrix} H_1\tilde{m}_0 \\ H_0\tilde{m}_1 \end{bmatrix}$$

$$\varepsilon_{01} = \lambda_{01} \left\langle \left(\mathbf{H}_0\mathbf{H}_1\right)^* \mathbf{H}_0\mathbf{H}_1 \right\rangle and\ \varepsilon_{10} = \lambda_{10} \left\langle \left(\mathbf{H}_1\mathbf{H}_0\right)^* \mathbf{H}_1\mathbf{H}_0 \right\rangle$$

It should be noted that the two regularization terms are equivalent in this case $\varepsilon_{01} = \varepsilon_{10}$.

Figure 1 Example of a Point Spread Function (PSF) grid from a generic model representing towed streamer acquisition (top) and OBN acquisition (bottom). Single PSFs are shown in both the depth domain (x,z) and wave number domain (Kx, Kz). The cross-survey PSF, shown in the far right, is used in the 4D joint reflectivity inversion.
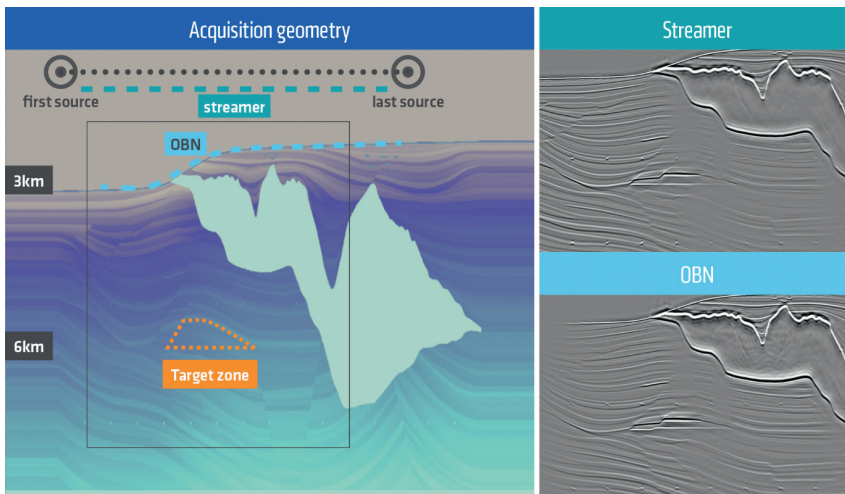
Figure 2 Model schematic for the 2D Sigsbee2B model indicating location of the reservoir target zone and the approximate positions of the towed streamer and OBN sensors. The corresponding migrated images using synthetics data for both surveys are displayed on the right hand side. The modeled 4D effect has been restricted to a single horizontal line corresponding to a vertical shift of the OWC at 6 km. No genuine 4D effects are expected above the OWC position.

The 4D reflectivity change is then given by $\Delta \hat{r} = \hat{r}_1 - \hat{r}_0$ for all systems.

The benefit of using XPSFs

Preconditioning the joint inversion system using the cross-survey Hessian gives rise to several advantages. Firstly, the regularization terms become symmetric, which helps to stabilize the inversion system. Secondly, the cross-survey Hessian represents the interaction between the wavefields of the different surveys involved. As with the standard Hessian, the diagonal of the cross-survey Hessian corresponds to the cross-survey illumination which can be interpreted as the multiplication of the base and monitor survey illuminations. If one of the surveys does not illuminate a particular reflector sufficiently than the cross-survey illumination becomes very small. In contrast, if the wavefields of the base and monitor are similar at the reflector then the cross-survey illumination is maximum.

Using the above described set-up, the cross-survey Hessian will be represented by a set of XPSFs which are derived from the PSFs that represent the imprint of the survey geometries of the baseline and monitor surveys on their respective subsurface illumination. The cross-survey PSFs (XPSFs) are effectively computed by Fourier domain multiplication of the Point Spread Functions of base and monitor survey (Figure 1). Consequently, wavenumbers present in both datasets are retained in the reflectivity inversion while wavenumbers, which are only present in one of the two datasets, are suppressed. As a result only the illumination common to both datasets is used to compute the changes in reflectivity caused by production effects.

Figure 1 illustrates how the PSF grids from two different surveys, one a Towed Streamer survey and one an OBN survey, are combined into a single set of XPSFs that enhance the common illumination from both geometries.

4D synthetic example 1: The Sigsbee2B model

The first 4D synthetic data example has been created using a subset of the Sigsbee2B 2D model. The 4D synthetic seismic data have been generated by modelling two different types of acquisitions, a streamer acquisition for the base survey and an OBN acquisition for the monitor survey (Figure 2 left hand side). The baseline towed streamer acquisition is modelled using 500 shots

with a shot point distance of 50 m and a 6000 m-long sensor cable with a receiver distance of 20 m. The monitor dataset has been modelled using the same shots geometry as for the base survey (i.e. a total of 500 shots) but the receiver network was composed of 120 OBNs positioned on the seabed 200 m apart from each other. The modelled 4D changes at the reservoir are characterized by a 40 m vertical shift of the position of the Oil Water Contact (OWC) and a velocity increase at the reservoir location of 10%.

Not much consideration was given to the magnitude of the 4D effects which are quite large as the study was purely focused on investigating the ability of the 4D reflectivity inversion to correct for all lateral illumination variations. It should be noted that no extra 4D processing steps were applied to the data pre- or post-imaging.

Figure 2 (right hand side) shows the migrated images for both the towed streamer and OBN acquisitions using the same velocity model. Because the survey geometries are distinctly different, attempting to compensate for the distortion to the resulting illumination using local scalars is not a successful option for extracting the true 4D signal at the reservoir.

The high values in the cross-survey illumination panel shown in Figure 3 define an area where the illumination of the two acquisitions has been very similar in amplitude. XPSFs provide an excellent opportunity for QC and to define areas with strong variations in local illumination between the different acquisitions such as the sub-salt part in the vicinity of the reservoir.

The reservoir has been purposely located beneath the salt body in an area of significant salt thickness variation. The aim is to evaluate the ability of the proposed cross-survey joint reflectivity inversion to recover the true 4D reflectivity without introducing unwanted artifacts which can be interpreted as 4D noise.

The results of the reflectivity inversion are presented in Figure 4 for two different inversion approaches. In the first approach a least-squares reflectivity inversion is carried out separately for both datasets. In the second approach the new joint reflectivity inversion process is applied.

The true 4D reflectivity response should be a single line (trough and peak) at the oil-water-contact (OWC) and a shift imprint below the OWC owing to the production induced velocity variation. Despite the very different acquisition geometries of

both base and monitor surveys, the inversion process in both cases has been able to recover a meaningful 4D reflectivity response. However, the separate inversion approach has resulted in more reflectivity artifacts around the OWC which are unrelated to the true 4D signal. It can be noted that diffraction points are visible in the reflectivity difference above and to the side of the main 4D effect. The joint inversion approach in contrast has produced results that show less artifacts especially in the area outside the reservoir where no production has occurred.

4D synthetic example 2: The SEAM time lapse model

The second synthetic example has been generated using the 3D/4D reservoir model provided by the SEAM time-lapse project (Oristaglio, 2016; Smit et al., 2017). Two different sets of 4D experiments with different OBN acquisition scenario have been tested in order to evaluate the capabilities of the 4D reflectivity inversion (Figures 5a and 5b). The first 4D OBN case involves two non-repeated survey geometries. The base survey design comprised 60 OBNs laid out in a rectangular shape and the monitor survey included two squares of 30 nodes each that are located to the side of the base survey. The second 4D experiment, which is used as an ideal reference case, comprises two exactly repeated sets of 180 nodes laid out in a 12 x 15 grid for both the base and monitor acquisitions.

The shot carpet was the same for all four receiver geometries. The geological model corresponds to a shallow water turbidite reservoir with the reservoir located at around 3500 m depth. A strong 4D difference is expected at the Gas-Oil contact at 3400 m depth owing to the large velocity variation as indicated in Figures 5c and 5d.

Figure 6 displays the 4D results for the non-repeated OBN acquisitions for depth slices at the water bottom (i.e. 260 m) and at the top of the reservoir (i.e. 3400 m). Figure 6a (left column) shows the 4D seismic difference results (i.e. straight seismic amplitude difference), Figures 6b and 6c (centre and right column) respectively show the separate reflectivity inversions and finally the joint reflectivity inversion results. At the water bottom it can be observed that the 4D difference around the node locations appear more focused and overall are of weaker amplitude once the reflectivity inversion is applied. However, the reflectivity differences do not cancel out for the separate reflectivity inversion cases as the individual illumination corrections are unconnected. In contrast, the jointly inverted reflectivity change (i.e. 4D reflectivity differences) becomes negligibly small at the water bottom; a consequence of the use of the cross-survey PSFs.

The bottom row of images in Figure 6 represent the 4D differences as estimated at the top of the reservoir. The 4D signal is partially imaged by the seismic amplitude difference and presents large lateral amplitude variations. The separate
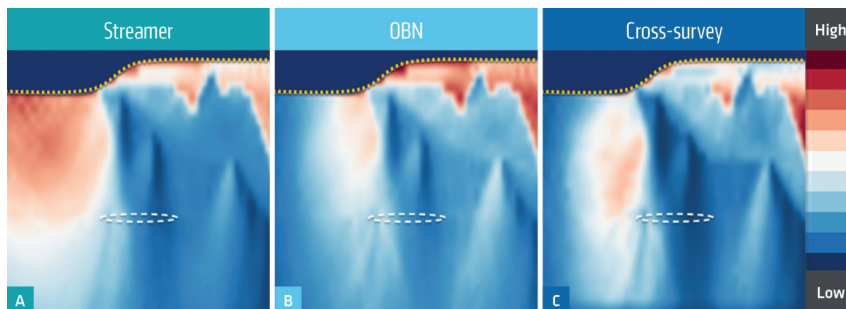

Figure 3 Total illumination panels for A) the towed streamer survey, B) the OBN survey and C) the combination of both surveys (i.e. cross-survey illumination).
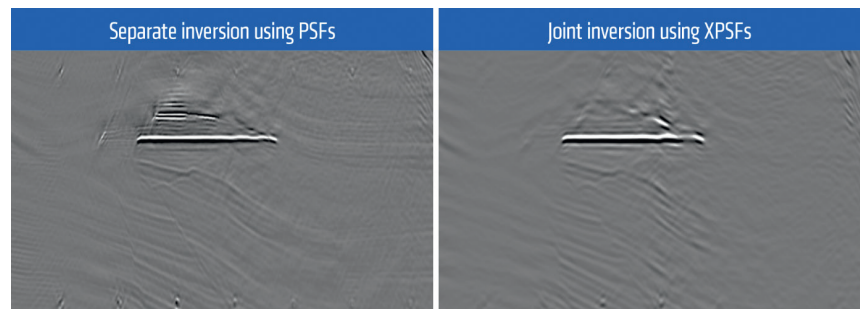
Figure 4 Resulting 4D reflectivity difference at OWC for the case of the separate application of PSFs to each time-lapse survey (left) and the joint application of cross-survey PSFs (right). Separate inversion approach shows more 4D noise above the OWC location than the joint reflectivity inversion.
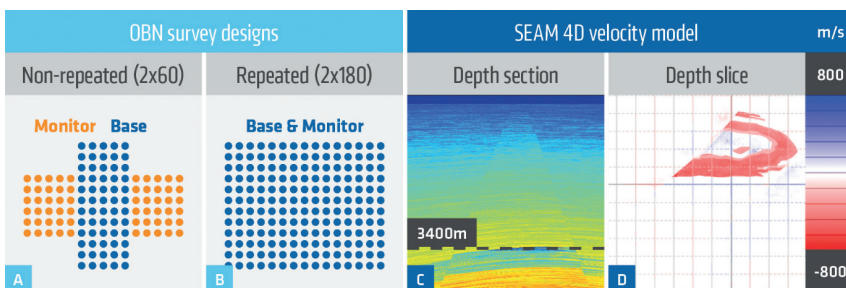

Figure 5 A) OBN node positions for non-repeated 4D survey. B) OBN node position for a perfectly repeated 4D survey. C) Velocity model section from the 3D SEAM model with the position of the top reservoir indicated by the dotted line. D) Depth slice through 4D SEAM velocity model at the top of the reservoir (i.e. 3400 m).
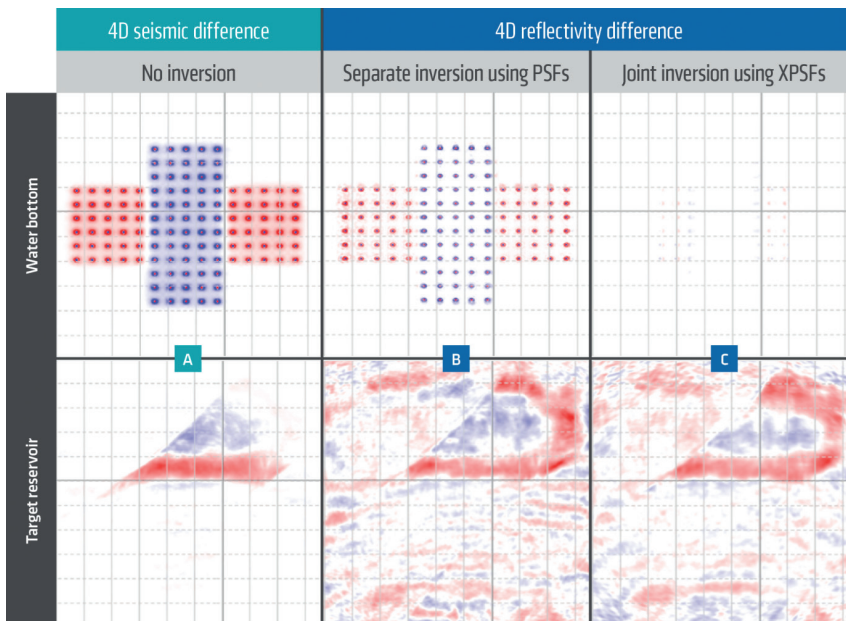
Figure 6 Upper panel represents a depth slice through the 4D difference cube at the water bottom position for the non-repeat OBN surveys. A) shows the result if no reflectivity inversion is applied, B) for the case where separate inversions are applied to each of the two vintages and C) the results for the joint reflectivity inversion of both base and monitor survey. The lower panel shows the result at the reservoir level.

Figure 7 Depth slice at the top of the reservoir for the perfectly repeated 4D OBN synthetic example. A) 4D difference when no reflectivity inversion is applied. B) 4D difference for the joint reflectivity inversion of both base and monitor. C) 4D velocity difference from the SEAM model for comparison with the reflectivity inversion results.
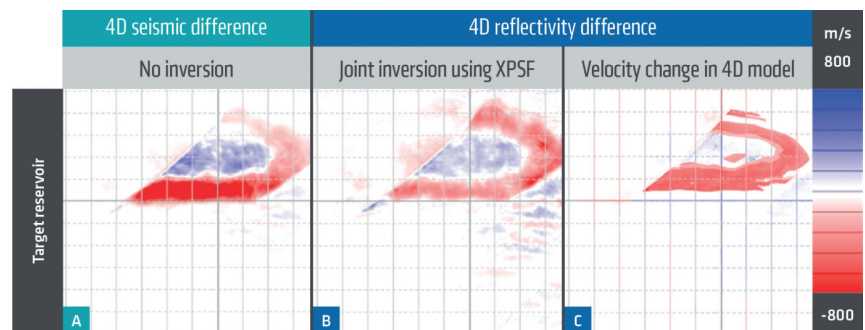
reflectivity inversions have improved the 4D signal but the lack of 4D constraint has over-boosted the 4D noise outside and inside of the 'D shaped' reservoir area. The joint reflectivity inversion by contrast was able to reduce the illumination-induced 4D noise further and enable the recovery of a 4D signal amplitude with the same geometry as the original 4D velocity model (Figure 5d).

These results have to be compared with the reference best case scenario, where the two OBN survey acquisitions are perfectly repeated (Figure 7). In this case, no illumination variation occurs between the base and monitor survey and the spatial amplitude variation of the 4D signal is purely owing to the distortion effects of the overburden geology and the limited aperture of the receiver and shot layout. Nevertheless, the joint reflectivity inversion results (Figure 7b) demonstrate the ability of the new 4D imaging workflow to recover the 4D amplitude differences very accurately and to produce a 4D image of higher resolution. The overall 4D noise level has been reduced compared to the results shown in Figure 6c but it should be noted that a total of 180 nodes were used for this best case scenario as compared to the 60 nodes for the case of non-repeated geometries.

Conclusion

Image domain 4D reflectivity inversion using multi-dimensional PSFs has been shown to be able to compensate for significant illumination differences when substantially different survey geometries are used for 4D imaging. The proposed methodology is particularly advantageous in 4D studies where the geometry of the different acquisitions cannot be replicated. This is likely be the case when towed streamer surveys with different acquisition directions are used in a 4D experiment or when streamer and OBN (Ocean Bottom Node) surveys are combined.

As shown using synthetic data examples, the joint reflectivity inversion process delivers improved results when compared to the use of separate inversions as it ensures a more robust recovery of the 4D effects and results in lower 4D noise. The presented new methodology using cross-survey Point Spread Functions (XPSFs) ensures consistency in the wavefields of the different time-lapse surveys and does not require additional constraints.

The 4D synthetic data examples shown here use models that produce strong and easy-to-detect 4D signals. If much smaller and more subtle 4D effects need to be recovered it will be paramount to repeat the acquisition geometries between the different time-lapse surveys as closely as possible.

The joint inversion methodology using XPSFs described here, however, will still be beneficial when applied to repeat sparse surveys of largely similar geometry. Combining the new 4D imaging inversion technique with an optimum 4D repeated acquisition design will be preferred when subtle 4D effects are to be detected.

Acknowledgements

constructive discussions during this project and PGS management for its approval to publish this work.

References

Ayeni, G. and Biondi, B. [2010]. Target-oriented joint least-squares migration/inversion of time-lapse seismic data sets. *Geophysics*, **75** (03), R61-R73.

Haacke, R.R., Casasanta, L., Hou, S. and Henderson J.R. [2017]. Dip-angle image filtering for 4D processing of towed-streamer and OBN datasets. *First EAGE Workshop on Practical Reservoir Monitoring*, Extended Abstracts, Th PRM 07.

Lecerf, D., Boelle, J.L., Lafram, A. and Cantillo, J. [2010]. WAZ Mirror Imaging with Nodes for Reservoir Monitoring - Dalia Pilot Test. *72nd EAGE Conference and Exhibition*, Extended Abstracts, D003.

Oristaglio, M.L. [2016]. SEAM Update: Integrated reservoir and geophysical modelling: SEAM Time Lapse and SEAM Life of Field. *The Leading Edge*, **35** (10), 912-915.

Smit, D., Oppert, S., Stefani, J., Artus, V., Herwanger, J., Popov, P., Bottrill, A., Tan, L., Hu, W., Liu, J., Abriel, W., Detomo, R., Barkhouse, W., and Oristaglio, M.L. [2017]. Large scale numerical simulation of reservoir monitoring – SEAM Time Lapse. *First EAGE Workshop on Practical Reservoir Monitoring*, Extended Abstracts, Th PRM 13.

Theriot, C., Wong, W.F. and Corcoran, C. [2015]. Qualitative 4D: matching ocean bottom seismic to towed streamer data. *85th SEG Annual Meeting*, Expanded Abstracts, 5461-5465.

Valenciano, A.A., Biondi, B., and A. Guitton [2006]. Target oriented wave-equation inversion. *Geophysics*, **71** (04), A35-A38.